Journal of
Applied Crystallography

ISSN 0021-8898

Received 4 November 2000
Accepted 3 February 2001

Microstructural transformation of vanadium pentoxide powder obtained by high-energy vibrational ball-milling

Partha Chatterjee,[a]† S. P. Sen Gupta[a]* and Suchitra Sen[b]

[a]Department of Materials Science, Indian Association for the Cultivation of Science, Jadavpur, Calcutta 700032, India, and [b]Central Glass and Ceramics Research Institute, Jadavpur, Calcutta 700032, India. Correspondence e-mail: msspsg@mahendra.iacs.res.in

An X-ray powder profile analysis of vanadium pentoxide powder milled in a high-energy vibrational ball-mill is presented. The strain- and size-induced broadening of the Bragg reflection for two different crystallographic directions ([001] and [100]) were determined by Warren–Averbach (WA) analysis, using a pattern-decomposition method assuming a pseudo-Voigt function. The deformation process causes a decrease in the domain size, and a near isotropic saturation value of ~10 nm is reached after severe milling. The initial stages of milling produce a propensity for size broadening, whereas, with increasing milling time, microstrain broadening is predominant. WA analysis indicated significant plastic strain along with spatial confinement of the internal strain fields, probably in the crystallite interfaces. Transmission electron microscopy revealed a drastic change in particle shape after 64 h of milling, indicating the existence of size anisotropy which, however, decreased with further increase of the milling time.

1. Introduction

Vanadium pentoxide is of current interest as an oxidation catalyst and as a thermally activated electrical and optical switching material. The material is a wide-band-gap semiconductor at room temperature and exhibits a metal–insulator transition at 530.5 K. It is now accepted that nanostructured materials have a wider application for their exceptional properties with respect to their bulk counterpart. Most of the work on V_2O_5 is limited to nanostructures in two-dimensional thin-film form (Rubin Aita *et al.*, 1986; Oh *et al.*, 1992). In this paper, we have concentrated on the nanostructure that is developed in three-dimensional form, *i.e.* in powder formed by high-energy vibrational ball-milling.

The investigation of the development of this nanostructure by different analytical techniques, such as surface-area measurement by the Brunauer–Emmett–Teller (BET) method, line-profile analysis by X-ray diffraction (XRD), and microstructure analysis by transmission electron microscopy (TEM), constitutes the main aim of our study.

X-ray diffraction line-profile analysis based on the Warren–Averbach (WA) method (Warren & Averbach, 1950) does not yield reliable results for the highly diffuse peaks with considerable overlapping often found in ball-milled samples. A very useful alternative to such numerical Fourier transformation is the profile-fitting/pattern-decomposition technique (*e.g.* de Keijser *et al.*, 1983; Langford *et al.*, 1986). It is now well established that X-ray diffraction lines may be modelled by a Voigt function. In our method we have considered a pseudo-Voigt function (Wertheim *et al.*, 1974) which provides a relatively better flexibility and consumes less computation time.

In addition to the determination of the size of coherently diffracting domains and lattice microstrains, the dependence on the coherence length L of the mean-square strain ($\langle\varepsilon_L^2\rangle$) obtained from WA analysis provides useful information regarding the nature of strain fields. A useful interpretation of the mean-square strain curves is possible on the basis of the concept of local strains and spatial variation of the mean-square strain (indicating non-uniform strains in the diffracting columns) (Turunen *et al.*, 1983) and has been followed in the present work.

2. Experiment and data analysis

V_2O_5 powder of purity 99.6% and initial particle size 0.5 μm (Aldrich, USA) was dry ball-milled in Al_2O_3 cretoid with a single Al_2O_3 ball of diameter ~1.5 cm, for different lengths of time (from 8 h to 250 h) in a SPEX 8000 Mixer Mill (Glen Creston Ltd, UK). In order to minimize the effect of heating due to long hours of milling, an indigenously made timer was used which switched the ball-mill on and off alternately every half hour (Chakraborty & Sen, 1995).

The X-ray diffraction pattern of the as-milled powder specimen was recorded in a Philips PW1710 diffractometer operating at 35 kV and 20 mA using Ni-filtered Cu $K\alpha$ radiation in a step-scan mode with a step size of 0.02° 2θ and a dwell time varying from 2 to 10 s per step to obtain a good signal-to-noise ratio for a reliable profile-fitting application. Polycrystalline defect-free Si [see van Berkum *et al.* (1995) for details] powders were used for instrumental broadening correction.

The surface area of the ball-milled powder was measured by the single-point BET method by nitrogen adsorption in a surface-area analyzer (Carlo Erba Strmentazione, Italy). TEM was performed at 120 kV in a Jeol 200 kV transmission electron microscope.

† Present address: Department of Physics, Vivekananda Mahavidyalaya, Haripal, Hooghly 712405, India.

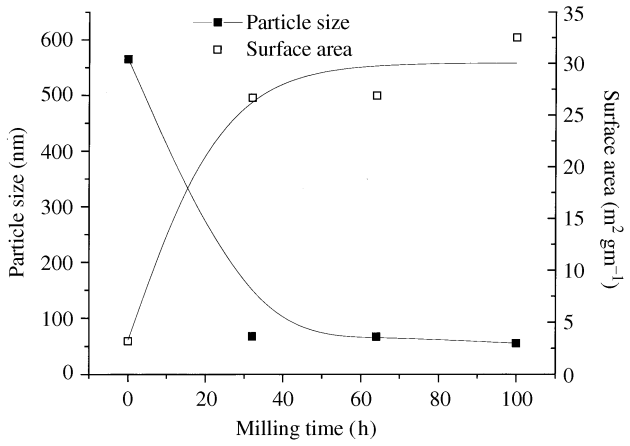

Figure 1
Variation of surface area and particle size of V_2O_5 powders from BET measurements.

The X-ray diffraction line profile was assumed to be a pseudo-Voigt function defined as

$$\mathrm{pV}(2\theta) = I_0[\eta L(2\theta) + (1-\eta)G(2\theta)], \quad (1)$$

where

$$L(2\theta) = \left\{1 + \left[(2\theta - 2\theta_0)/\omega\right]^2\right\}^{-1}, \quad (2)$$

$$G(2\theta) = \exp\left\{-(\ln 2)\left[(2\theta - 2\theta_0)/\omega\right]^2\right\}, \quad (3)$$

η is the Lorentzian content, I_0 is the intensity maximum of the $k_{\alpha 1}$ peak, $2\theta_0$ is the Bragg angle, and ω is the half width at half-maximum. An asymmetric function,

$$A(2\theta) = \exp\left[-a\left|(2\theta - 2\theta_0)/\cot 2\theta_0\right|\right], \quad (4)$$

is also convoluted with the above pV function to include the effect of asymmetry originating at low angles due to axial divergence in the instrumental profile recorded with an Si sample.

The above function, along with a linearly varying background, is fitted to the X-ray diffraction profiles, and the parameters related to the profile shape are extracted using an algorithm developed by Enzo *et al.* (1988).

The Fourier transform of a symmetric pseudo-Voigt function is given by

$$F(L) = \left[(1-\eta)(\pi/\ln 2)^{1/2}\exp\left(-\pi^2\omega^2L^2/\ln 2\right) + \eta\pi\exp(-2\pi\omega L)\right]. \quad (5)$$

Subsequently, the size–strain separation was performed on the basis of the WA method.

3. Results and discussion

3.1. Surface-area measurement

An important visual observation was made of the ball-milled V_2O_5 powder. In the finely divided state, V_2O_5 powder is yellow in colour. With milling, the shade slowly changes, *i.e.* from deep yellow after 8 h of milling to brown after 150 h of milling. This change in the optical properties in turn indicates a change in oxidation state of vanadium. This will require a more exhaustive investigation of the chemical structural state by X-ray photoelectron spectroscopy in the future.

The surface area of the unmilled and milled powder was measured by the BET technique. The particle size was calculated from the measured surface area assuming sphericity of powder particles. A significant increase in the surface area and the consequent reduction in particle size was observed with milling, as is evident from Fig. 1. The particle size reduces to about 50 nm after 100 h of milling.

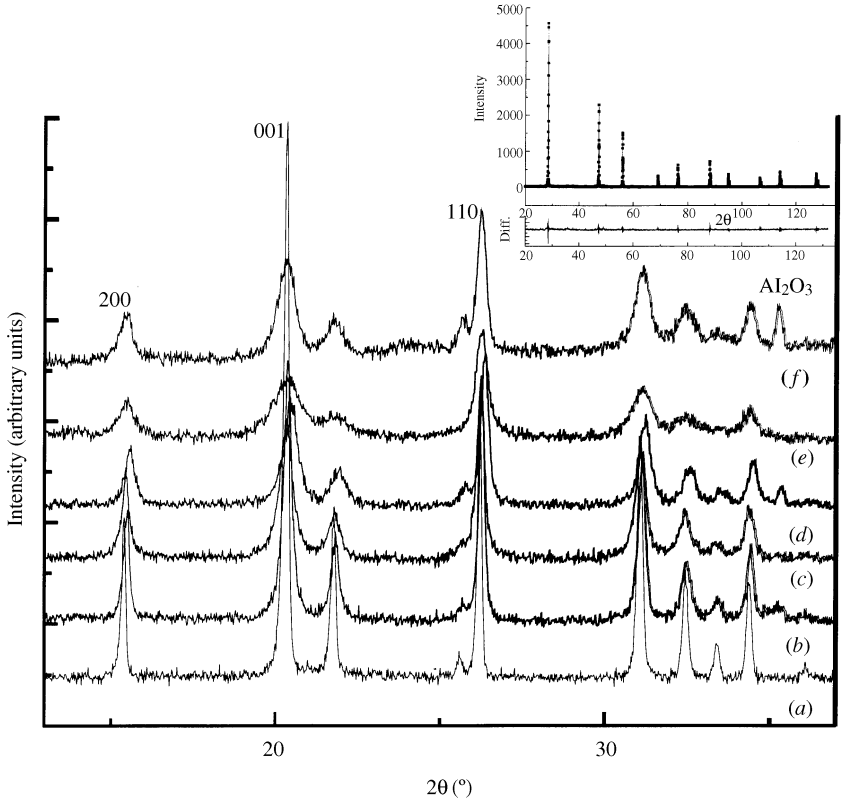

Figure 2
XRD patterns of the milled samples (only a portion is shown). (*a*) Unmilled, (*b*) 16 h, (*c*) 32 h, (*d*) 100 h, (*e*) 150 h, (*f*) 250 h. The inset shows a fitted Si pattern.

3.2. X-ray diffraction

Fig. 2 shows the evolution of XRD patterns of the V_2O_5 samples milled for increasing times. Reasonably symmetric peaks justify the application of equation (1) as a fitting function for V_2O_5 reflections. Considerable broadening of the XRD lines, supplemented by reduction of intensity, illustrates the effect of heavy deformation on the milled samples. Both the [100] and [001] directions are rapidly affected for the initial hours of milling, with the least effect in the [110] direction. This indicates a comparatively easy reduction of crystallite size along the *a* and *c* orthogonal axes.

The presence of Al_2O_3 peaks (from ball and vial) can be noticed after 32 h of milling. The lattice parameter measurements, however, do not indicate considerable contamination of the samples from vial and ball. The values of the cell parameters are quoted in Table 1.

Table 1
Variation of lattice parameter with milling time.

Milling time (h)	a (±0.008–0.01 Å)	b (±0.005–0.008 Å)	c (±0.005–0.008 Å)
0	11.510 (11.51†)	3.563 (3.559†)	4.371 (4.371†)
8	11.455	3.545	4.354
16	11.496	3.560	4.368
32	11.506	3.562	4.375
64	11.496	3.563	4.368
100	11.470	3.550	4.362
150	11.493	3.561	4.363
200	11.486	3.558	4.361
250	11.487	3.560	4.375

† Reported value PDF 9-387.

3.3. Line-broadening analysis

In our procedure of two-stage analysis, first the profile shape parameters are obtained through a pattern decomposition, followed by a multiple-order WA method for size–strain separation for both the [100] and the [001] direction. A qualitative description of the operative cause of line broadening is presented on the basis of the variation of the profile shape parameter Φ ($= 2\omega/\beta$, 2ω = FWHM, β = integral breadth) (Langford, 1992). For initial milling times (up to 32 h) the Lorentzian content of the profile increases rapidly indicating the fracture of the powder particles due to repeated ball–powder impact and reflecting the size broadening as an operative cause for overall line broadening. For longer milling times (>32 h) the Gaussian content increases (up to 150 h) with the milling time, indicating the propensity for strain broadening. A further decrease in the shape factor is noticed for samples milled beyond 150 h, which probably indicates further decrease in the crystallite size and relaxation of the lattice microstrains.

In our analysis all three available orders for the [100] direction (200–400–600) are used. It is observed that $\ln A_L$ varies linearly with d^{*2}, suggesting that the size–strain separation according to the WA method is fairly reliable and yields acceptable results. The size Fourier coefficients did not reveal any systematic 'hook' effect; the coherent domain size calculated therefrom for the two different crystallographic directions [100] and [001] are quoted in Table 2. It is observed that the domain size decreases rapidly during the initial hours of milling and attains a saturation value of ∼10 nm at higher milling times. The difference in the values of the domain sizes for the two directions indicates size anisotropy up to ∼150 h of milling. After 200 h of milling, however, the crystallites assume an isotropic size at least in the above two crystallographic directions. These results are in conformity with the ball-milled metallic samples (Hellstern *et al.*, 1989; Lutterotti & Gialanella, 1997), where a similar behaviour of the crystallite size with milling time was observed.

The value of the volume-weighted crystallite size D_v is obtained from the $A_s(L)$ curve according to the equation

$$D_v = 2 \int A_s(L)\, \mathrm{d}L, \qquad (6)$$

and is given in Table 2. The volume-weighted crystallite size also decreases with the milling time. Discrepancies in some cases are due to uncertainty in the size Fourier coefficients (as D_v is sensitive to the shape of the A_S curve). The ratio $D_v/D_{\rm eff}$ for milling times less than 100 h is less than, but close to, 2, indicating that the size-broadened profile is, in general, Voigt in nature with more weight towards Lorentzian content (Balzar & Ledbetter, 1993). Furthermore, it is observed that, for milling times up to 32 h, the ratio increases, establishing that the operative cause of overall line broadening for milling times less than 32 h is size broadening. The above ratio, however, decreases after 100 h of milling and reaches the value of an ideal Gaussian size-broadened profile.

The decrease of the mean-square strain obtained for the [100] and [001] directions with L is physically interpreted in terms of local strain $\langle \varepsilon_0^2 \rangle$ and its derivatives in order to understand the nature of strain fields (Turunen *et al.*, 1983). Considering the spatial fluctuation of mean-square strains, the following expression for the mean-square strains is generally obtained:

$$\langle \varepsilon_L^2 \rangle = \langle \varepsilon(z)^2 \rangle - \frac{\langle \varepsilon'(z)^2 \rangle L^2}{12} + \frac{\langle \varepsilon''(z)^2 \rangle L^4}{360} - \frac{\langle \varepsilon'''(z)^2 \rangle L^6}{20160}, \qquad (7)$$

where z is the coordinate in crystal space. The above equation is fitted to the mean-square microstrain curves with a total of 12 parameters. The local mean-square strain and mean-square strain derivatives are given in Table 2. Only the first derivative is given, which is often sufficient to explain the results. Fig. 3 shows the variation of the local mean-square strain, the strain derivative and the inverse of volume-weighted column length with milling time along the [100] direction. It is observed that for smaller milling times (<32 h) the volume-weighted crystallite size decreases rapidly (see $1/D_v$ *versus* t plot in Fig. 3*b*). Beyond 32 h of milling, the local strain and mean-square derivative increase rapidly and reach a maximum after 150 h of milling, indicating an increased non-uniformity in the diffracting columns with milling time. The decrease in the microstrain and strain derivatives beyond 150 h indicates a relaxation of strain. Similar behaviour is observed along the [001] direction (see Table 2). It is also clear from Fig. 3 that perhaps strains are much higher in smaller domains or crystallites, indicating short-ranged strain fields. It is interesting to note that the level of plastic strain is similar to that often found in heavily deformed metallic samples (Hellstern *et al.*, 1989; Wagner *et al.*, 1996). Measurement of lattice parameters provides a value of $\Delta a/a$ or $\Delta c/c$ that is too small and is not consistent with the microstrain measurements.

The above results presented for a ball-milled ceramic sample are not consistent with those of ball-milled metallic samples where the root-mean-square microstrain increases rapidly during the initial hours of milling, due to a large increase in the dislocation density, and then levels off as the material assumes nanocrystalline dimensions,

Table 2
Crystallite size and root-mean-square microstrain from WA analysis.

	[100]				[001]			
Milling time (h)	$D_{\rm eff}$ (±1–2 nm)	D_v (nm)	$\langle \varepsilon_0^2 \rangle^{1/2} \times 10^3$	$\langle \varepsilon_L'^2 \rangle^{1/2} \times 10^5$	$D_{\rm eff}$ (±1–2 nm)	D_v (nm)	$\langle \varepsilon_0^2 \rangle^{1/2} \times 10^3$	$\langle \varepsilon_L'^2 \rangle^{1/2} \times 10^5$
0	90	113	2.6 (5)	1.6 (5)	74	84	3.0 (5)	7.5 (6)
8	20	29	2.9 (5)	15.0 (11)	26	38	6.3 (12)	29.6 (24)
16	22	36	4.5 (6)	14.8 (9)	14	27	5.5 (9)	27.7 (24)
32	14	25	5.5 (10)	28.0 (23)	8	14	6.3 (9)	42.4 (30)
64	12	19	6.32 (10)	38.7 (26)	8	14	8.4 (12)	58 (4)
100	11	20	6.3 (11)	41 (3)	10	15	14.5 (26)	143 (11)
150	12	16	15.5 (20)	109 (7)	7	8	21.6 (30)	306 (20)
200	10	13	9 (1)	72 (4)	9	11	13.4 (18)	138 (9)
250	10	14	9.0 (11)	60 (3)	10	12	11.0 (17)	109 (8)

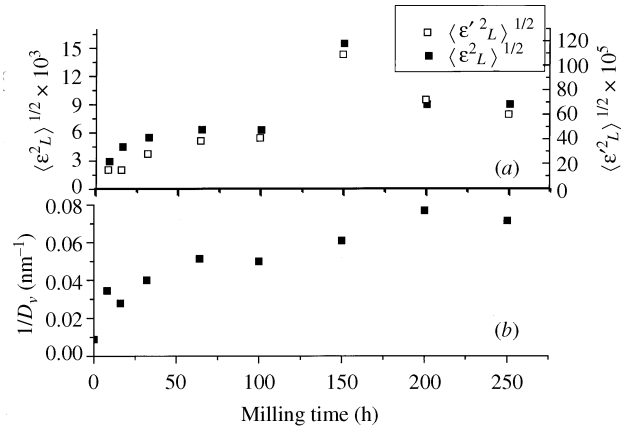

Figure 3
Variation of local mean-square strain, strain derivative and inverse of volume-weighted crystallite size D_v with milling time along [100].

where it is assumed that the energy supplied by ball-milling is not sufficient for a dislocation motion and hence further grain refinement is not possible. Although the variations of the root-mean-square microstrain with milling time are different, the variations of the mean-square strain with coherence length L are similar for both metallic and ceramic nanocrystals (Lutterotti & Gialanella, 1997; Reimann & Wurschum, 1997; Wagner *et al.*, 1996). A general conclusion can be derived from such results that crystallite or grain boundaries are disordered. Although high-resolution electron microscopy (HREM) studies indicate that the grain boundary structure is different for metals and oxides, a disordered boundary structure has been observed both in metallic (Thomas *et al.*, 1990; Wunderlich *et al.*, 1990) and in oxide nanocrystals (Rickerby, 1997). It has also been observed that the epitaxic grain boundary tends to occur less frequently in oxides than in metals (Ishida *et al.*, 1995). The presence of shear defects in nanocrystalline TiO_2 (Chang *et al.*, 1993) has also been found in the grain boundary regions and is explained as being due to an oxygen deficiency. In all cases, the width of the disordered region is small and extends up to a few nanometers only.

The method presented here in terms of microstrains and strain derivatives provides an alternative way of studying the extent of inhomogeneity and the nature of localization of strain fields in nanocrystalline materials.

3.4. TEM study

TEM observations (Figs. 4*a*–4*c*) show a somewhat similar structure. V_2O_5 unmilled powder shows irregular-shaped plate-like crystals. The selected area diffraction (SAD) pattern was analyzed and it was found to belong to V_2O_5 with an orthorhombic lattice. The average particle size was measured from the bright-field micrographs and was found to be ~200 nm. After milling for 64 h, the particle size reduces to ~50 nm. The plate-like morphology starts changing to irregular shapes with some crystals taking the form of elongated particles. This is more evident in powder milled for 100 h, where the major fraction takes the habit of elongated crystals (Fig. 4*a*), indicating size anisotropy. The diffuseness of the diffraction rings indicates a poor degree of crystallinity. This is also indicated in our XRD pattern and is consistent with our earlier observation of TiO_2 nanoparticles formed by the same method (Sen *et al.*, 1999). After 150 h of milling, particles of different morphology were observed, indicating inhomogeneity of the milled samples. Some, but not all, of the elongated particles drastically changed to a spherical habit (Fig. 4*b*), while some retained

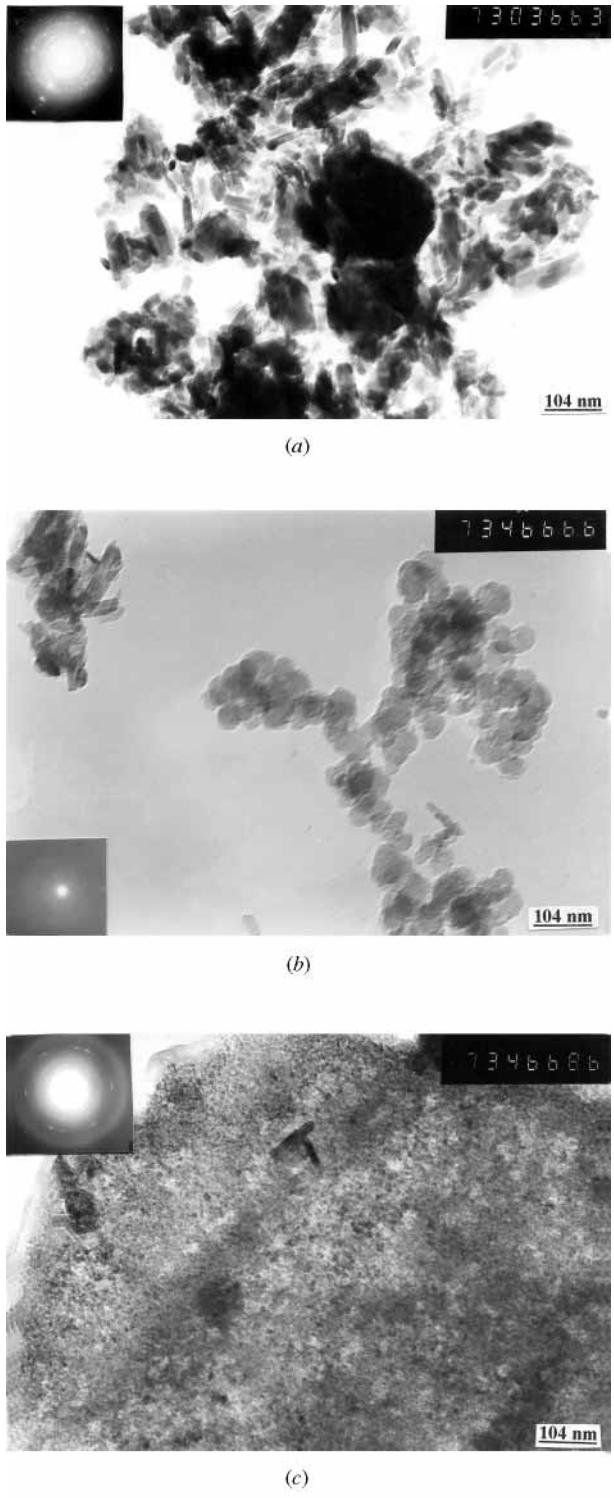

Figure 4
TEM micrographs and SAD patterns of ball-milled V_2O_5 powders. (*a*) 100 h, (*b*) 150 h, (*c*) 150 h.

their original elongated shape. This is quite interesting. In other regions, nanoparticles of size ~6 nm could be observed (Fig. 4*c*). The size reduction was not appreciable for spherical particles (~40 nm). After 200 h of milling, the TEM observations replicate the observation of the powder milled for 150 h (Fig. 4*b*). However, the more isotropic nature in particle shape indicates size isotropy too, which supports the XRD observation for isotropic particles; the average

size was found to be ∼30 nm. A final comparison with the XRD crystallite size and TEM particle size is possible on the basis of the assumption of spherical particles. Considering the value of D_v, the value of the particle diameter is about 4/3 of this value and the average is of the order of ∼20 nm for samples milled after 200 h, which is in agreement with the TEM value of 30 nm. Thus, a near one-to-one correspondence is observed from both XRD and TEM studies.

4. Conclusions

From the present study, the following conclusions can be made.

Ball-milling of V_2O_5 powder leads to the formation of nanocrystalline powders, along with a significant amount of plastic inhomogeneous strain.

The initial hours (<32 h) of milling lead to considerable grain refinement whereas microstrains are the prominent cause of line broadening at higher milling times.

The nature of the variation of microstrains with coherence length is similar to that obtained for metals. Increasing local strain and strain gradients in the diffracting columns with milling time indicates spatial confinement of stress fields.

Size anisotropy along [001] and [100] exists up to 150 h of milling. A narrow distribution of crystallite size, however, is obtained after 150 h of milling and isotropic crystallite size along both [001] and [100] is observed.

TEM studies support the XRD observations. A decrease of size anisotropy is evident in micrographs of powders milled for 150 and 200 h. Largely, the particles narrow down to ∼30 nm; this value agrees with the X-ray value of ∼20 nm.

The authors thank Mr M. L. Ram and Mr A. K. Ghosh of CGCRI, Calcutta, for experimental help in ball-milling the powder and for performing BET measurements, respectively. They are also thankful to RSIC, Bose Institute, for the TEM facility. One of the authors (SS) is grateful to Dr H. S. Maiti, Director, CGCRI, Calcutta, for his permission to publish this paper. The financial assistance of DST, Government of India, through grant No. III. 4(10)/93-ET during the course of the work is gratefully acknowledged. One of the authors (PC) also wishes to acknowledge CSIR, New Delhi, for the award of a Senior Research Fellowship.

References

Balzar, D. & Ledbetter, H. (1993). *J. Appl. Cryst.* **26**, 97–103.
Berkum, J. G. M. van, Sprong, G. J. M., de Keijser, Th. H., Delhez, R. & Sonneveld, E. J. (1995). *Powder Diffr.* **10**, 129–139.
Chakraborty, A. K. & Sen, S. (1995). CGCRI Internal Report No. IDMAC/007/95. CGCRI, Calcutta 700032, India.
Chang, W., Cosandey, F. & Hahn, H. (1993). *Nanostruct. Mater.* **2**, 29.
Enzo, S., Fagherazzi, G., Benedetti, A. & Polizzi, S. (1988). *J. Appl. Cryst.* **21**, 536–542.
Hellstern, E., Fecht, H. J., Fu, Z. & Johnson, W. L. (1989). *J. Appl. Phys.* **65**, 305–310.
Ishida, Y., Ichinose, H., Kizuka, T. & Suenaga, K. (1995). *Nanostruct. Mater.* **6**, 115.
Keijser, Th. H. de, Mittemeijer, E. J. & Rozendaal, H. C. F. (1983). *J. Appl. Cryst.* **16**, 309–316.
Langford, J. I. (1992). *Accuracy in Powder Diffraction II*, NIST Special Publication No. 846, edited by E. Prince & J. K. Stalick, pp. 110–126. Washington, DC: US Departmment of Commerce.
Langford, J. I., Loüer, D., Sonneveld, E. J. & Visser, J. W. (1986). *Powder Diffr.* **1**, 211–221.
Lutterotti, L. & Gialanella, S. (1997). *Acta Mater.* **46**, 101–110.
Oh, Y.-S., Watanabe, Y. & Takata, M. (1992). *J. Ceram. Soc. Jpn*, **100**, 1390.
Reimann, K. & Wurschum, R. (1997). *J. Appl. Phys.* **81**, 7186–7192.
Rickerby, D. G. (1997). *Philos. Mag. B*, **76**, 573–583.
Rubin Aita, C., Li Liu, Y., Kao, M. L. & Hansen, S. D. (1986). *J. Appl. Phys.* **60**, 749–753.
Sen, S., Ram, M. L., Roy, S. & Sarkar, B. K. (1999). *J. Mater. Res.* **14**, 841.
Thomas, G. J., Siegel, R. W. & Eastman, J. A. (1990). *Scr. Metall. Mater.* **24**, 201–206.
Turunen, M. J., de Keijser, Th. H., Delhez, R. & van de Pers, N. M. (1983). *J. Appl. Cryst.* **16**, 176–182.
Wagner, C. N. J., Yang, E. & Boldrick, M. S. (1996). *Nanostruct. Mater.* **7**, 1–11.
Warren, B. E. & Averbach, B. L. (1950). *J. Appl. Phys.* **21,** 595–599.
Wertheim, G. K., Butler, M. A., West, K. W. & Buchanon, D. N. E. (1974). *Rev. Sci. Instrum.* **11**, 1369–1371.
Wunderlich, W., Ishida, Y. & Maurer, R. (1990). *Scr. Metall. Mater.* **24**, 403–408.